Weather and Climate Extremes 46 (2024) 100729

Contents lists available at ScienceDirect

Weather and Climate Extremes

journal homepage: www.elsevier.com/locate/wace

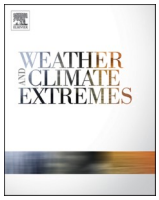

The 2022 record-high heat waves over southwestern Europe and their underlying mechanism

Jeong-Hun Kim [a,b], So-Hyun Nam [b], Maeng-Ki Kim [b,c,*], Roberto Serrano-Notivoli [d], Ernesto Tejedor [e]

[a] Earth Environment Research Center, Kongju National University, Gongju, 32588, South Korea
[b] Department of Atmospheric Sciences, Kongju National University, Gongju, 32588, South Korea
[c] Particle Pollution Research and Management Center, Gongju, 32588, South Korea
[d] Department of Geography and Regional Planning, Environmental Sciences Institute, University of Zaragoza, Zaragoza, Spain
[e] Department of Geology, National Museum of Natural Sciences-Spanish National Research Council (MNCN-CSIC), Madrid, Spain

ARTICLE INFO

Keywords:
Heat waves
Southwestern Europe
Iberian Peninsula
Blocking events
Extreme events

ABSTRACT

Recently, the intensity and frequency of heat waves (HWs) have been increased worldwide. Particularly in 2022, Europe was severely affected by unprecedented HWs, which caused approximately 61,672 deaths and 11,324 deaths in Europe and Spain, respectively. In this study, we investigate the mechanisms of the HWs in southwestern Europe (SWEU) to identify the differences between typical HWs and the extreme HWs that occurred in 2022. Our results showed that the SWEU events in 2022 were strongly related to robust heat domes that developed in the lower troposphere due to high-pressure anomalies especially during two periods (9–18 June and 8–19 July). Analyses of the energy budget and thermodynamic equation revealed the processes underlying the amplification of the heat domes over SWEU during both periods. We also discovered that abnormal atmospheric blocking in the upper troposphere was closely associated with the amplification of the Gulf Stream SST, which caused an atmospheric circulation pattern favorable for the 2022 SWEU-HWs. This was further confirmed by modeling experiments. Therefore, our results emphasize that a Gulf Stream SST amplification can trigger an atmospheric circulation pattern favorable for extreme HWs in SWEU, enhancing our understanding of the mechanism behind extreme HWs. Finally, our findings will help improving the forecasting of SWEU-HWs on a sub-seasonal time scale, as well as future projections in global climate models.

1. Introduction

Global warming, which is rapidly intensifying, leads to extreme events and changes in climate variability, causing severe socio-economic damage. As a result of global warming, the frequency and intensity of heat waves (HWs) in mid-latitudes and Europe are clearly increasing (Rousi et al., 2022; Vautard et al., 2020). The 2003 summer HW in Europe caused over 70,000 deaths from heat-related complications, demonstrating the vulnerability of European countries to heat exposure (Robine et al., 2008). In 2022, southwestern Europe (SWEU), including the Iberian Peninsula (IP), experienced the highest average summer temperature in 900 years (Büntgen et al., 2024), and northeastern Spain experienced the driest summer in 279 years (Serrano-Notivoli et al., 2023). During the 2022 SWEU-HWs, temperatures in Portugal rose to above 47 °C in July, causing severe damage, including 1 063 excess mortality deaths from heat-related illnesses, according to Portugal's Directorate-General for Health. The human toll across Europe was even more staggering, with over 60,000 heat-related deaths reported in the summer of 2022, most notably in Italy and Spain (Tejedor et al., 2024). Hence, there is an increasing interest in the underlying causes of HWs over the IP and SWEU.

SWEU-HWs are affected by various factors (Barriopedro et al., 2023;

Abbreviations: CLIM, climatological mean; CTRL, control runs; DLW, downward longwave radiation; HW, heatwave; HWY, HW year; NA, North Atlantic; SNAO, summertime NA oscillation; SST, sea surface temperature; SSTexp, SST perturbed runs; SWEU, southwestern Europe; TMN, minimum temperature; TMX, maximum temperature; WAF, wave activity flux.

* Corresponding author. Department of Atmospheric Sciences, Kongju National University, Room 443, Natural Science Building (#11), 56 Gongjudaehakro, Gongju, 32588, South Korea.
E-mail address: mkkim@kongju.ac.kr (M.-K. Kim).

https://doi.org/10.1016/j.wace.2024.100729
Received 25 June 2024; Received in revised form 24 September 2024; Accepted 30 September 2024
Available online 1 October 2024

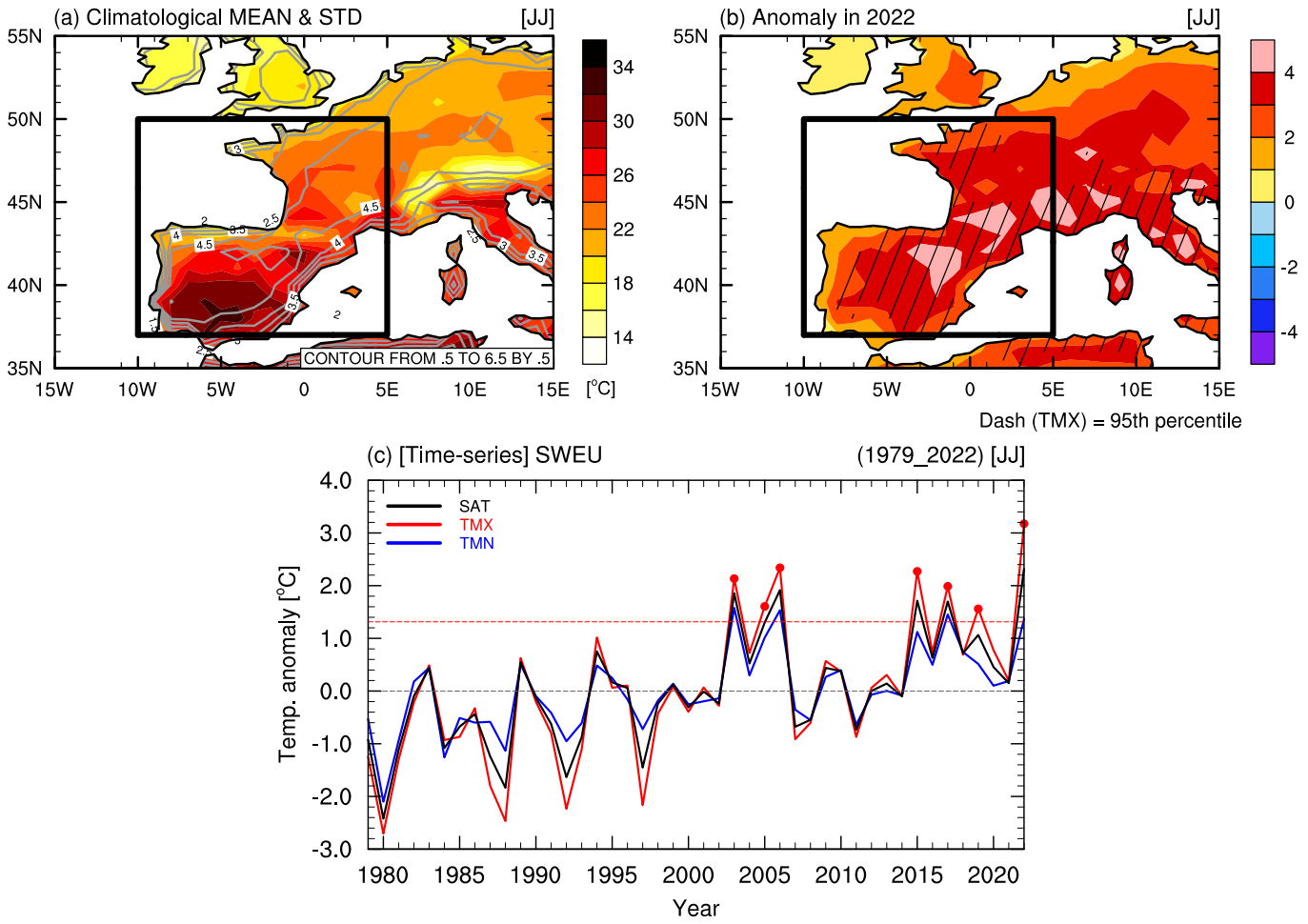

Fig. 1. (a) Climatological means (shaded) and standard deviations (contours) of the TMX (unit: °C) from June to July (JJ) during 1979–2022. (b) Anomaly pattern of TMX in JJ 2022. The black rectangle indicates the area of the SWEU. The black dashed pattern denotes above the 95th percentile for the analysis period. (c) Time series of the TMX (red solid line) in the black rectangle area in (b) and standard deviations of TMX (dashed line). The solid red circles indicate HWYs in the black rectangle area in Fig. 1(a) and (b). (For interpretation of the references to color in this figure legend, the reader is referred to the Web version of this article.)

Garcia-Herrera et al., 2010a; Tomczyk et al., 2017). Using a convolutional neural network deep learning model, Son et al. (2022) revealed that European summers have lengthened over the past 42 years. They also suggested that the intensification of mid-latitude jet streams associated with topographical effects in Greenland accelerates global warming, leading to the earlier onset of summers and, consequently, more frequent HWs across Europe. In fact, due to global warming, the frequency, intensity, and duration of HWs in mid-latitudes and Europe are clearly increasing (Bento et al., 2022; Rousi et al., 2022). Serrano--Notivoli et al. (2022) reported that HWs have occurred more frequently in Spain since the early 1980s and that the number, duration, and intensity of events are remarkably increasing.

HWs in European regions are influenced by upper-troposphere blocking, increased sea surface temperature (SST), and decreased soil moisture (Garcia-Herrera et al., 2010a; Liu et al., 2020; Seo et al., 2019). Upper-troposphere blocking events affecting European HWs are thought to occur due to the weakening of the meridional temperature gradient, which reduces the strength of mid-latitude jet stream and facilitates the development of stationary high-pressure systems that cause HWs. These blocking events, resulting from the weakened jet stream, have been identified as the causes of significant HW episodes in Western Europe (in 1994, 2003, 2006, 2010, 2017, and 2018) (Barriopedro et al., 2011; Rousi et al., 2022; Sánchez-Benítez et al., 2018). Yet, Duchez et al. (2016) demonstrated that the HW in Western Europe in 2015 was associated with SST anomalies in the North Atlantic (NA). In fact, a significant meridional temperature gradient in the NA-SST can induce stagnation in the upper-troposphere jet stream, which in turn leads to an inflow of cold air over the NA and of warm air over Western Europe, promoting the development of stagnant high pressures and extreme HWs in the Western European region. Stéfanon et al. (2014) estimated that a reduction in soil moisture was responsible for up to 20% of the temperature anomaly in western Europe during HWs. When soil moisture is low, reduced evaporation leads to less cooling and, consequently, higher temperatures, a critical factor in climate interactions and projections (Seneviratne et al., 2010). It results in a feedback via land–atmosphere interaction, leading to an increase in the persistence of HW days. There was an important water deficit in the IP in the months prior to June as both winter and spring had been arid in 2022 (Toreti et al., 2023). May was also scorching, the warmest on record, with a positive anomaly of 2.5 °C over the peninsula of Spain (Tripathy and Mishra, 2023). It undoubtedly contributed to a persistent dry and warm soil and atmosphere that, together with the water deficit of the previous months, set the ground for enhancing the June and July HWs.

While Serrano-Notivoli et al. (2023) focused primarily on the role of the NA blocking event in channeling hot air from Africa to the IP, our study further explores the dynamical mechanisms behind the persistence of the blocking pattern itself. Specifically, we investigate the associated Rossby wave and their interactions with the atmospheric circulation, providing deeper insights into the drivers of the prolonged HW in 2022. Despite the numerous studies on SWEU-HWs, the physical causes of exceptionally severe HWs such as those experienced in 2022 and the fundamental mechanisms triggering such patterns remain

unclear. Therefore, here we investigated the distinctive atmospheric circulation patterns associated with the 2022 SWEU-HW compared to typical HW characteristics in SWEU. Additionally, we aimed to identify the drivers of the temperature increase in SWEU and the underlying causes of the atmospheric circulation patterns that led to these extreme heat events.

2. Data and methods

2.1. Reanalysis data on HWs and atmospheric circulations

HWs and associated atmospheric circulation patterns over the SWEU were investigated using European Center for Medium-Range Weather Forecasts (ECMWF) Reanalysis Data Version 5 (ERA5) from 1979 to 2022 (Hersbach et al., 2020). The horizontal and vertical resolutions of the ERA-5 data used in this study were 1° × 1° and 37 levels, respectively. Daily anomalies were calculated by eliminating daily climatological means of 44 years (1979–2022) from the daily values. May 2022 was scorched and the warmest on record (instrumental), with a positive anomaly of 3 °C over the peninsula of Spain. It undoubtedly contributed to a persistent dry and warm soil and atmosphere, which set the ground for enhancing the June and July HWs together with the previous months' water deficit. Therefore, this study mainly focused on June to July 2022, when the record-breaking HWs occurred. The daily maximum temperature (TMX) and minimum temperature (TMN) were calculated using 1-hourly surface air temperature (i.e., 2-m air temperature) data.

To further investigate the cause of increasing temperature, the SWEU region (10 °W –5 °E and 37 °N –50 °N; black rectangle in Fig. 1) has been selected as the target region. Compared to the rest of the country, the study area exhibits high climatological mean TMX, with significant positive TMX anomalies, especially in 2022.

2.2. Budget of the thermodynamic energy equation

The atmospheric apparent heat source term, diabatic heating (Q_1), was calculated using the thermodynamic energy equation and residual term reported by Yanai et al. (1973) (Eq. (1)). Specifically, all necessary variables (U, V, ω, T) were obtained from the ERA5 reanalysis dataset, ensuring that the computed values are derived directly from observed atmospheric data rather than model-generated outputs. This method involves solving the equation for Q1 as a residual, as shown in Eq. (2), incorporating radiative heating, latent heat release from net condensation, and surface heat fluxes redistributed by unresolved mixing processes.

$$\frac{\partial T}{\partial t} = -\vec{V} \bullet \nabla T + \left(\frac{p}{p_0}\right)^{\frac{R}{c_p}} \omega \frac{\partial \theta}{\partial p} + \frac{Q_1}{c_p} \quad \text{(Eq. 1)}$$

where T, $\vec{V}$, ω, and p represent the air temperature, horizontal wind, vertical pressure velocity, and pressure, respectively. The constants p_0 and c_p in this equation are the reference pressure (1 000 hPa) and specific heat of dry air at constant pressure (1004 $Jkg^{-1}K^{-1}$), respectively. The local change term ($\partial T/\partial t$) is influenced by the horizontal advection term ($-\vec{V} \bullet \nabla T$), adiabatic term ($\left(\frac{p}{p_0}\right)^{\frac{R}{c_p}} \omega \frac{\partial \theta}{\partial p}$), and diabatic heating term (Q_1/c_p). After rearranging to solve for Q1, the residual form is represented in Eq. (2):

$$Q_1 \Big/ c_p = \left[\frac{\partial T}{\partial t} + \vec{V} \bullet \nabla T - \left(\frac{p}{p_0}\right)^{\frac{R}{c_p}} \omega \frac{\partial \theta}{\partial p}\right] \quad \text{(Eq. 2)}$$

Using ERA5 data, Q_1 was computed as a residual without relying on model outputs of Q_1 itself.

2.3. Wave activity flux

To confirm the propagation of Rossby wave energy, we analyzed the wave activity flux (WAF), a vector quantity representing the propagation of Rossby wave energy in the atmosphere (Takaya and Nakamura, 2001b). WAF is useful for diagnosing the propagation paths of stationary Rossby waves, allowing for a better understanding of how these waves influence climate patterns. It provides a means to visualize the direction and intensity of Rossby wave propagation, especially in the analysis of centers of action where atmospheric blocking or persistent weather patterns are observed (Kim et al., 2019, 2022). Analyzing the WAF, we can identify Rossby wave energy transport from one region to another, thereby gaining insights into the mechanisms driving large-scale climate variability. We calculated the three-dimensional WAF using the following equation suggested by Takaya and Nakamura (2001b):

$$\mathbf{W} = \frac{p\cos\phi}{2|\mathbf{U}|} \begin{pmatrix} \frac{U}{a^2\cos^2\phi}\left[\left(\frac{\partial\psi'}{\partial\lambda}\right)^2 - \psi'\frac{\partial^2\psi'}{\partial\lambda^2}\right] + \frac{V}{a^2\cos\phi}\left[\frac{\partial\psi'}{\partial\lambda}\frac{\partial\psi'}{\partial\phi} - \psi'\frac{\partial^2\psi'}{\partial\lambda\partial\phi}\right] \\ \frac{U}{a^2\cos\phi}\left[\frac{\partial\psi'}{\partial\lambda}\frac{\partial\psi'}{\partial\phi} - \psi'\frac{\partial^2\psi'}{\partial\lambda\partial\phi}\right] + \frac{V}{a^2}\left[\left(\frac{\partial\psi'}{\partial\phi}\right)^2 - \psi'\frac{\partial^2\psi'}{\partial\phi^2}\right] \\ \frac{f_0^2}{N^2}\left\{\frac{U}{a\cos\phi}\left[\frac{\partial\psi'}{\partial\lambda}\frac{\partial\psi'}{\partial z} - \psi'\frac{\partial^2\psi'}{\partial\lambda\partial z}\right] + \frac{V}{a}\left[\frac{\partial\psi'}{\partial\phi}\frac{\partial\psi'}{\partial z} - \psi'\frac{\partial^2\psi'}{\partial\phi\partial z}\right]\right\} \end{pmatrix} + \boldsymbol{C}_u\boldsymbol{M}, \quad \text{(Eq. 3)}$$

where p and a are the pressure and mean radius of the Earth, respectively. $\psi', \phi,$ and λ represent stream function anomalies, latitude, and longitude, respectively. The basic flow is $\mathbf{U} = (U, V, 0)^T$, phase propagation in the $\mathbf{U}$ direction is $\boldsymbol{C}_u = \left(\frac{U}{|\mathbf{U}|}C_p, \frac{V}{|\mathbf{U}|}C_p, 0\right)^T$, and wave-activity pseudo momentum is $\boldsymbol{M} = \frac{p}{2}\left(\frac{q'^2}{2|\nabla_H\mathscr{Q}|} + \frac{e}{|\mathbf{U}|-C_p}\right)\cos\phi$. C_p, e, and q' represent the gas constant of dry air, perturbation of the wave energy, and quasi-geostrophic potential vorticity, respectively. We analyzed WAF to confirm that Rossby wave propagation was responsible for the HWs in the SWEU. For further details on the WAF equations, refer to Takaya and Nakamura (2001b) (the WAF code is available at https://www.atmos.rcast.u-tokyo.ac.jp/nishii/programs/index.html).

2.4. Modeling experiments

To support our findings, we performed climate modeling experiments using the Community Atmospheric Model version 5 (CAM5) within the Community Earth System Model version 1.2.2 (CESM v1.2.2) developed by the US National Center for Atmospheric Research. The CAM5 model was configured with a finite volume dynamical core with a horizontal resolution of 1.9° × 2.5° and 30 vertical levels extending to 3 hPa (~40 km). We ran two equilibrium experiments: control (CTRL) and SST perturbed (SSTexp) runs. The experiments only differed in the surface boundary conditions over the NA. SST anomalies in the NA region were prescribed from June to July 2022, when the warming signals were significant. For areas other than the NA, we prescribed the climatological mean SST from 1979 to 2022. We integrated the model experiments for 120 years and analyzed the last 100 years to confirm the model response to SST anomalies changes in NA in an equilibrium state. The modeled atmospheric response to SST warming over the NA region was defined as the difference between the means of the SSTexp and CTRL runs, and a two-tailed Student's *t*-test was used to determine the significance of the difference.

Table 1
Rank of the HWs in the SWEU over 44 years from 1979 to 2022. Anomaly with respect to the climatological mean in parentheses.

Heat wave Years	2003	2005	2006	2015	2017	2019	2022
TMX (°C)	27.77 (+2.13)	27.24 (+1.60)	27.98 (+2.33)	27.91 (+2.27)	27.63 (+1.98)	27.20 (+1.56)	28.81 (+3.17)
Rank	4	6	2	3	5	7	1

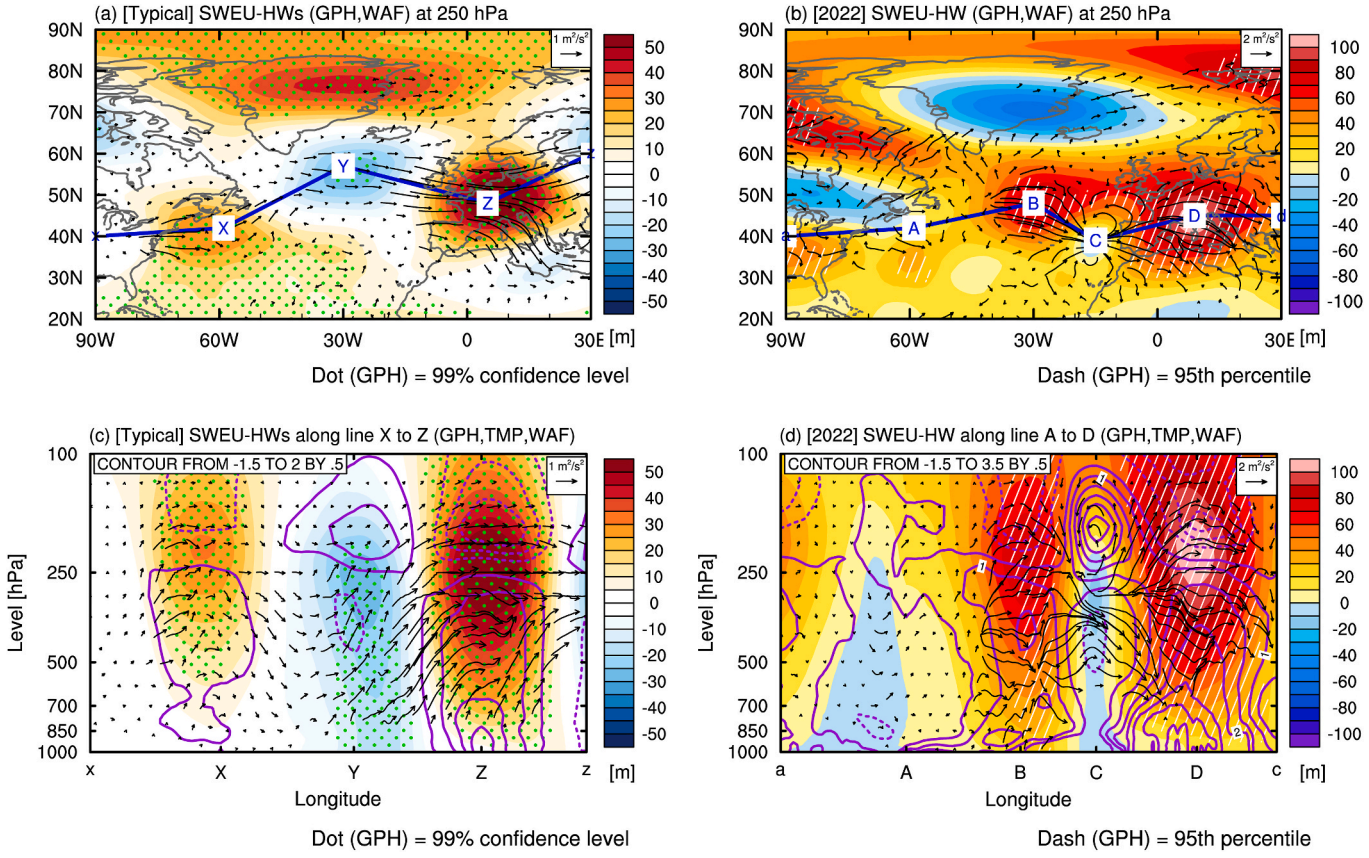

Fig. 2. (a) and (c) Horizontal and vertical composite patterns for geopotential height (GPH; shaded; unit: m), WAF (vector; unit: m^2/s^2), and air temperature (TMP; purple line; unit: °C) for typical SWEU-HWs. (a) The solid blue line indicates a Rossby wave pathway, and the dotted area denotes statistically significant values at 99% level. (b) and (d) The same as in panels Fig. 2(a) and (c), but for 2022 SWEU-HW. (b) The white dashed patterns denote above the 95th percentile of GPH at 250 hPa for the analysis period. (For interpretation of the references to color in this figure legend, the reader is referred to the Web version of this article.)

3. Results

3.1. Characteristics of the SWEU-HWs

Fig. 1 shows the climatological characteristics of SWEU-HWs. The climatological mean and standard deviation of the daily mean TMX over SWEU are high during the early summer (June and July), at 25.64 °C and 3.48 °C, respectively (Fig. 1a; black rectangle). The 2022 TMX anomalies in the SWEU region exceeded the 90th percentile, indicating the occurrence of at least one extreme HW out of ten (Fig. 1b). According to the interannual variability in the average TMX in the SWEU region, which showed high variability, the TMX in the SWEU region was steadily increasing (Fig. 1c). This study, therefore, defines HW years (HWYs) as a year during the analysis period when the daily TMX in the SWEU region was more than +1 standard deviation above the climatological mean TMX, and are shown in Table 1. Typical HWYs are defined as the average of years excluding 2022. HWYs mainly occurred after 2000, possibly because of global warming and/or Atlantic multidecadal oscillation. In particular, the 2022 HW was exceptional and unlike the previous HWs. It featured an unprecedented TMX of 28.81 °C (3.17 °C over than climatological mean). Meanwhile, HWYs were identified using two timeseries: one that includes the trend and one that excludes the trend. Even when trends were removed, 2003, 2005, 2006, 2015, and 2022 consistently emerged as typical HWYs. This indicates that the classification of these years as HWYs is robust, irrespective of trend considerations. The anomaly patterns observed in HWYs without the trend are closely consistent with those observed in years with the trend, suggesting that the presence or absence of a trend does not significantly impact the identification of extreme HWYs (figure not shown). This indicates that the classification of these years as HWYs is robust, irrespective of trend considerations. In this study, subsequent analyses considered HWYs with the trend included.

Next, we investigated in which aspects the unprecedented 2022 HWs differed from previous HWs. To do so, we examined the atmospheric circulation patterns with distinct characteristics of HWs occurring in SWEU (Fig. 2). The predominant occurrence of typical SWEU-HW patterns revealed that they are associated with Rossby wave patterns in the upper troposphere (Fig. 2a–c). These Rossby wave atmospheric circulation patterns, originating in the upstream regions, induced favorable barotropic high-pressure anomalies conducive to HW development over Europe, passing through the western NA and Iceland. In contrast, the atmospheric circulation features during the 2022 HW differed significantly from the typical SWEU-HW patterns (Fig. 2b–d). During the 2022 SWEU-HW, expansive high-pressure anomalies formed in the upper

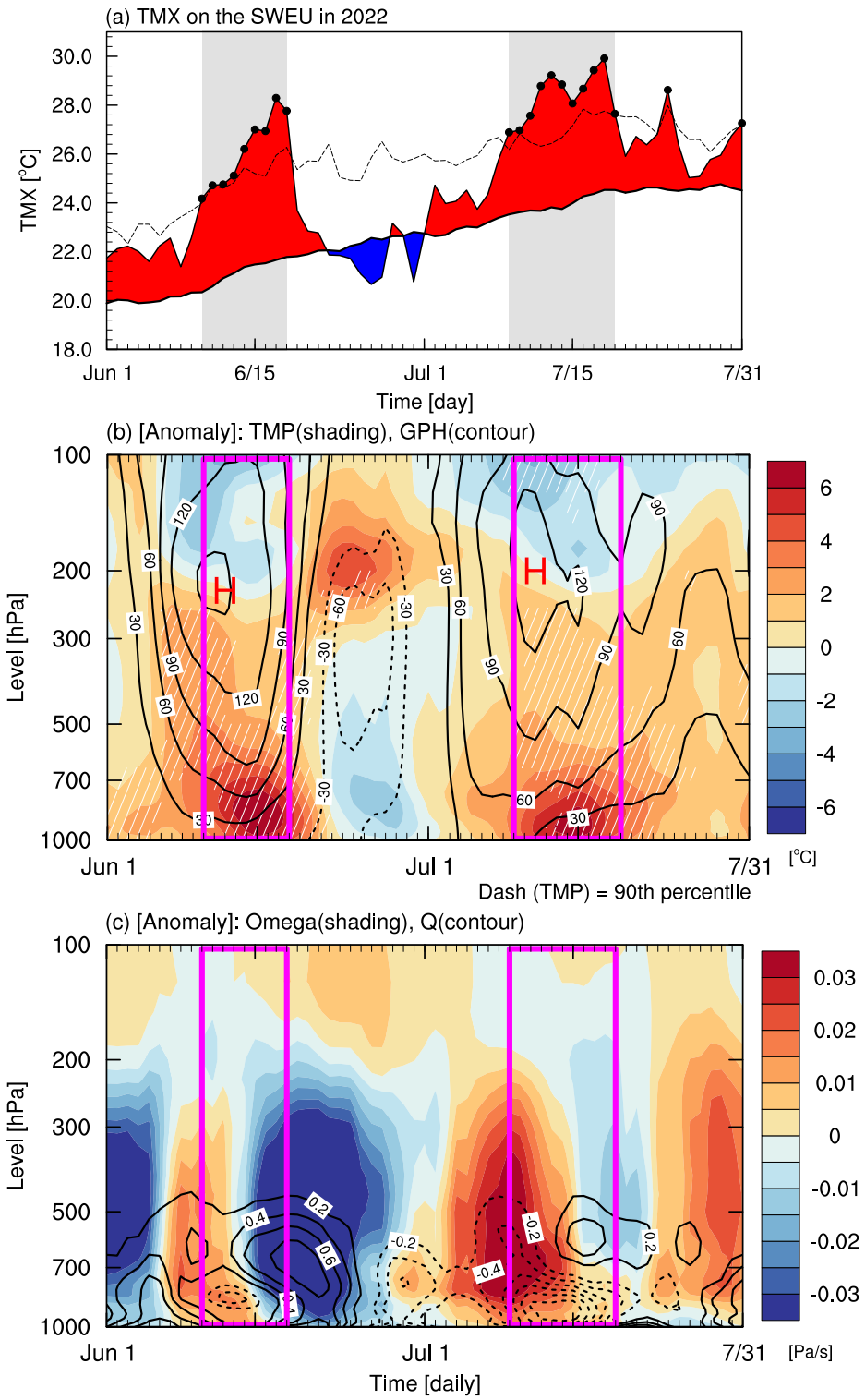

Fig. 3. (a) Time series of TMX on the SWEU in 2022. The black dotted line indicates the daily mean TMX in 2022. The thick black solid line and gray dashed line indicate the climatological mean and 95th percentile for the analysis period, respectively. Gray-shaded periods represent P1 (10–18 June) and P2 (9–18 July). (b) Spatio-temporal changes in daily temperature (TMP; shaded; unit: °C), geopotential height (GPH; black contour; unit: m), (c) omega (shaded; unit: Pa/s), and specific humidity (Q; contour; unit: g/kg) at 1 000–100 hPa in JJ 2022. The white dashed patterns denote above the 90th percentile for the analysis period. Pink rectangles indicate P1 and P2. (For interpretation of the references to color in this figure legend, the reader is referred to the Web version of this article.)

troposphere, stretching from the NA to the European continent. Furthermore, the NA and SWEU regions showed significant warming from the surface to the upper troposphere. These findings implied that the 2022 extreme HW in SWEU occurred through mechanisms distinct from those of typical SWEU-HWs.

3.2. Physical mechanism of the 2022 SWEU-HW

To examine the spatio-temporal variability in the 2022 SWEU-HW, we investigated atmospheric variable changes during June and July (Fig. 3). TMX values exceeded the 95th percentile of TMX during 10 days

Table 2
Thermodynamic energy budget in P1 and P2, integrated over the lower troposphere (1 000−850 hPa), expressed in units of K/day. Climatological means (CLIM) are shown in parentheses, representing the average values over the entire analysis period, covering both P1 and P2.

	P1 (CLIM)	P2 (CLIM)	P1 anomaly	P2 anomaly
Local change	0.387 (0.171)	0.229 (0.113)	0.216	0.115
Horizontal advection	−0.945 (−1.362)	−1.676 (−1.795)	0.416	0.119
Adiabatic heating	0.616 (0.448)	1.016 (0.613)	0.167	0.402
Diabatic heating (Q1)	0.717 (1.084)	0.889 (1.295)	−0.367	−0.406
Units: K/day				

Table 3
Surface energy budget in P1 and P2, expressed in units of W/m^2. Positive and negative values denote downward and upward flux, respectively. Climatological means (CLIM) are in parentheses.

	P1 (CLIM)	P2 (CLIM)	P1 anomaly	P2 anomaly
Net SW	268.728 (248.001)	282.873 (251.311)	20.726	31.562
Net LW	−80.248 (−72.306)	−91.4327 (−75.734)	−7.941	−15.698
SHF	−35.779 (−30.155)	−39.045 (−35.012)	−5.623	−4.033
LHF	−63.485 (−66.962)	−60.035 (−66.714)	3.477	6.679
DLW	349.807 (337.033)	352.088 (349.262)	12.774	2.825
Units: W/m^2				

from 10 to 19 June and 11 days from 9 to 19 July (Fig. 3a). The TMX recorded during these two periods exceeded the 95th percentile of the daily TMX, which ranges with the criteria for extended HWs rather than only being classified as extreme based on one standard deviation. In fact, during this extended HW period, the TMX in SWEU reached its highest value of 29.91 °C on July 18th, 2022. We labeled these two periods with consistently higher temperatures than the 95th percentile of TMX for more than 5 day as P1 (10–19 June) and P2 (9–19 July). Next, we analyzed temporal changes in vertical atmospheric variables during P1 and P2. In both periods, high-pressure anomalies developed, including barotropic structures in the upper and lower troposphere, before the HW started (Fig. 3b). In addition, the air temperature in the lower troposphere increased significantly, and a heat dome persisted during both periods. The specific humidity in the lower troposphere exhibited markedly different patterns during the two periods (Fig. 3c). While positive specific humidity anomalies were observed during P1, negative anomalies were evident during P2. Humidity plays a crucial role in controlling atmospheric temperature through several physical processes, with the presence or absence of moisture significantly impacting air temperatures. During P1, positive specific humidity anomalies likely enhanced latent heat release via condensation, thereby increasing air temperatures. In contrast, negative humidity anomalies during P2 could have reduced latent heat release, resulting in less atmospheric warming. This difference underscores the importance of moisture availability in influencing temperature dynamics. Fischer and Schär (2010) further elaborated that limited soil moisture reduces evaporative cooling, which can amplify HW events by sustaining high temperatures. Similarly, Miralles et al. (2014) noted that increased atmospheric humidity diminishes the effectiveness of surface heat dissipation, contributing to heat stress and higher air temperatures. This is particularly relevant in regions like Southern Europe, where moisture dynamics play a vital role in the development and persistence of HWs. This implies that the significantly developed heat domes during both periods may have been caused by different physical processes associated with the moisture in each period. In P2, the specific humidity did not increase significantly, which implies that the atmosphere was hot and dry. These results indicate that the temperatures of the warm and moist air in P1 and the hot and dry air in P2 in the lower troposphere were distinctly increased and persisted for an extended period as a heat dome.

To determine the cause of the increased air temperature in the lower troposphere in SWEU, we analyzed the thermodynamic equation budget (Table 2). Climatologically, in P1 and P2, the temperature in the SWEU region was affected by cold advection and balanced with adiabatic and diabatic heating. The high-pressure anomalies across SWEU in 2022 caused strong subsidence, increasing adiabatic heating and balancing horizontal temperature advection and diabatic heating. As a result, the lower troposphere air temperature in both periods was mainly increased by anomalous warm advection and adiabatic heating due to the high-pressure anomaly. However, the causes of the temperature increases differed between P1 and P2. During P1, the temperature increased mainly because of horizontal advection, whereas during P2, it increased because of adiabatic heating. This implies that the increased temperatures in both periods were affected by different processes.

Then, we analyzed the surface energy budget and anomaly patterns over the SWEU region to further investigate the increased surface temperatures during P1 and P2 (Table 3, Fig. 4a and b). During both periods, a high-pressure anomaly over SWEU increased shortwave radiation, and increased shortwave radiation energy is mainly dissipated through longwave radiation and sensible heat flux. However, latent heat flux did not increase, which implies that evaporation from the surface did not increase. Climatologically, winds from the Atlantic Ocean dominate the SWEU region in summer (Fig. 4a and b). During both periods, the increase in air temperatures in the lower troposphere was mainly influenced by reduced cold air advection from the ocean and intensified warm air advection from the African continent (Fig. 4a and b). However, during P1 and P2, the surface and lower-troposphere wind speed decreased, which may explain the lack of dramatic changes in the sensible and latent heat fluxes.

During P1, the increased specific humidity in the SWEU region led to higher downward longwave radiation (DLW) in the lower troposphere, contributing to rising air temperatures. This increased specific humidity promoted positive water vapor feedback according to the Clausius–Clapeyron relation, further amplifying temperature increases. The enhanced specific humidity during the P1 was primarily due to favorable atmospheric circulation patterns that promoted moisture advection into the region (Fig. 4c and d). Moreover, persistent anticyclonic conditions during this period likely enhanced land-atmosphere interactions, increasing local evaporation and maintaining high humidity. These combined effects created warm and moist atmospheric conditions that supported the development and maintenance of the heat dome, resulting in a prolonged HW. During P2, there was no apparent increase in moisture. Dry and hot atmospheric conditions and strong anticyclonic anomalies directly affected the strengthening and maintenance of the heat dome and caused the extreme HWs. In other words, the heat domes developed and were maintained due to the strong high-pressure anomaly and the atmospheric conditions being moist and warm during P1, and dry and warm during P2.

Next, we investigated what may have caused the atmospheric circulation patterns associated with the unusually intense 2022 SWEU-HW. Fig. 5 shows the atmospheric circulation patterns during P1 and P2. During these periods, broad anticyclonic anomalies strongly developed in the upper and lower troposphere in SWEU and the IP region, but their intensity and location differed. During P1, the center of the anticyclonic anomaly was located from the NA to SWEU (Fig. 5a–c). This atmospheric pattern resembles the summertime NA oscillation (SNAO) (pattern correlation between P1 and SNAO at 1000 hPa $= 0.609$; $p < 0.01$). However, the atmospheric circulation pattern during P1 was stronger than the typical SNAO pattern, and the center of activity developed relatively broadly to the south. According to Folland et al. (2009), if the SNAO index is substantially higher than normal, it is possible that temperatures will be higher in parts of northwestern Europe, whereas in

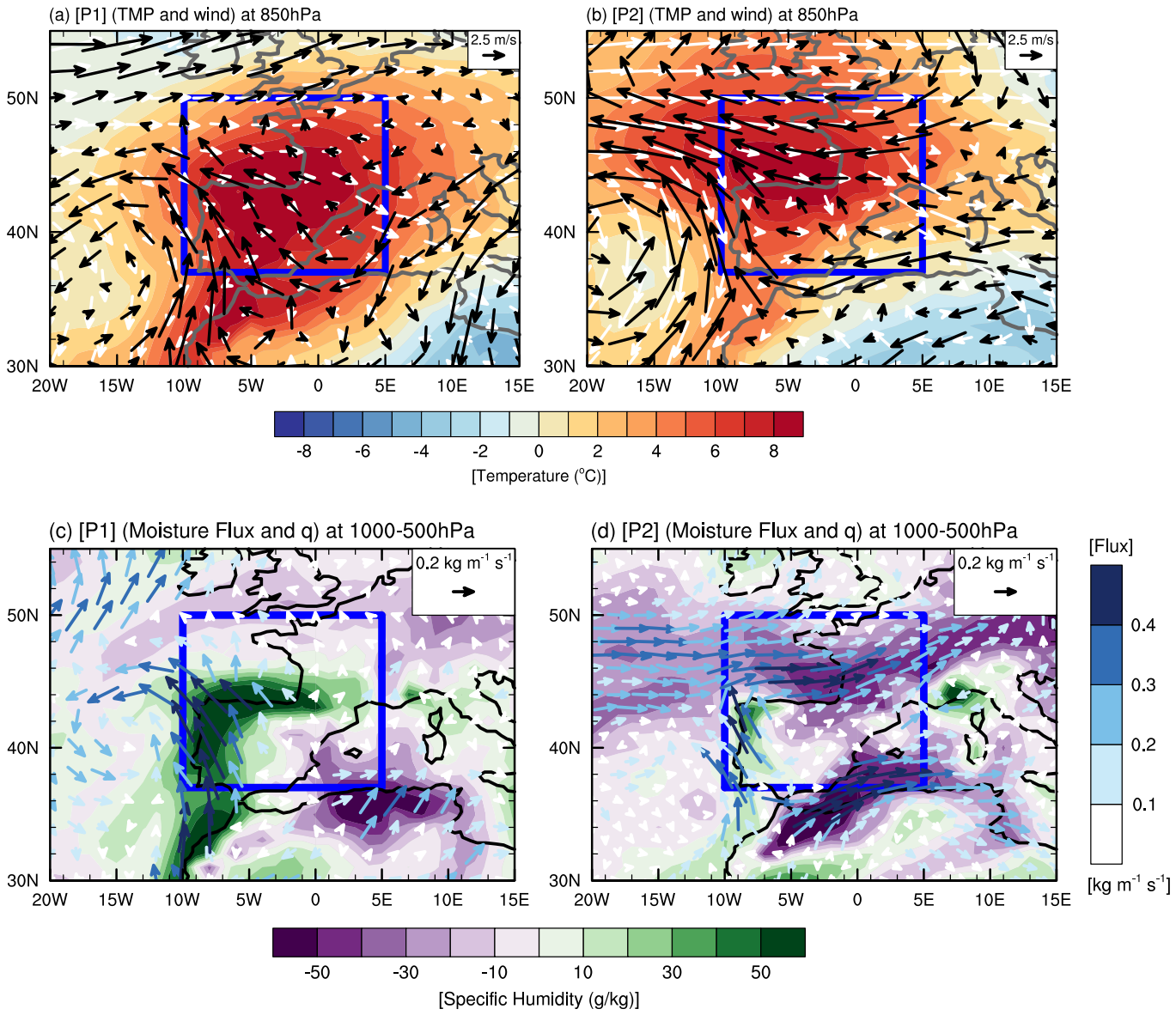

Fig. 4. (a-b) Anomaly patterns of wind (vectors; units: m s^{-1}) and air temperature (shading; units: °C) at 850 hPa during the (a) P1 and (b) P2 periods. White vectors in (a) and (b) represent the climatological mean wind vectors. (c-d) Anomaly patterns of moisture flux (color vectors; units: kg m^{-1} s^{-1}) and specific humidity (shading; units: g/kg) integrated over the 1 000−500 hPa during the (c) P1 and (d) P2 periods. The blue rectangles indicate the SWEU region. (For interpretation of the references to color in this figure legend, the reader is referred to the Web version of this article.)

the Mediterranean and southern regions, temperatures will be lower than normal, and precipitation more likely to decrease. However, in this case, the SNAO index was higher than 0.5 standard deviations during P1 (0.520), yet there was an extreme SWEU-HW. Therefore, its relationship with the SNAO must be studied in depth and perhaps reevaluated in the future.

During P2, the anticyclonic anomaly was located toward the UK, a relatively northern region as compared to that in P1, and appeared to be strong and broad (Fig. 5d–f). During P2, the positive SNAO did not appear clearly, and the atmospheric circulation pattern was typical of a blocking stationary anticyclone. Therefore, the atmospheric patterns during P1 and P2 were mainly affected by the development of unusually robust atmospheric blocking patterns, which were stronger than those in previous HWs. This atmospheric blocking and ridge-type atmospheric circulation drives the Central-European HWs (Sousa et al., 2018).

Li et al. (2020) suggested that the combined impact of positive NAO and atmospheric blocking triggered the 2018 HWs in Europe. This atmospheric blocking pattern extends from the Gulf Stream on the east coast of North America to Europe. The expansion of the Gulf Stream is crucial in regulating climate, weather patterns, and atmospheric blocking (Simmonds and Govekar, 2014). Therefore, we analyzed the SST in the NA to determine the cause of atmospheric blocking during the 2022 SWEU-HW (Fig. 6). The results showed that the SST patterns during a typical SWEU-HW and the 2022 SWEU-HW are dramatically different (Fig. 6a and b). During a typical SWEU-HW, warm SSTs appeared throughout the NA (Fig. 6a). However, during the 2022 SWEU-HW, the SST in the Gulf Stream and the Mediterranean Sea increased (Fig. 6b). The warm SST anomalies in the Mediterranean Sea and the Arctic Ocean are shown similarly in the typical SWEU-HWs; these features may be a result of the strongly developed high-pressure anomaly. The most notable feature of the SST in 2022 SWEU-HW was the significant increase in warm SST anomalies in the Gulf Stream. These characteristics appear similarly in the P1 and P2 periods. However, compared to the P1, the Gulf Stream was more extended in the central NA during the P2 period (Fig. 6c and d). The P2 pattern is more similar to the 2022 SWEU-HW SST anomalies. The warm SSTs in the Gulf

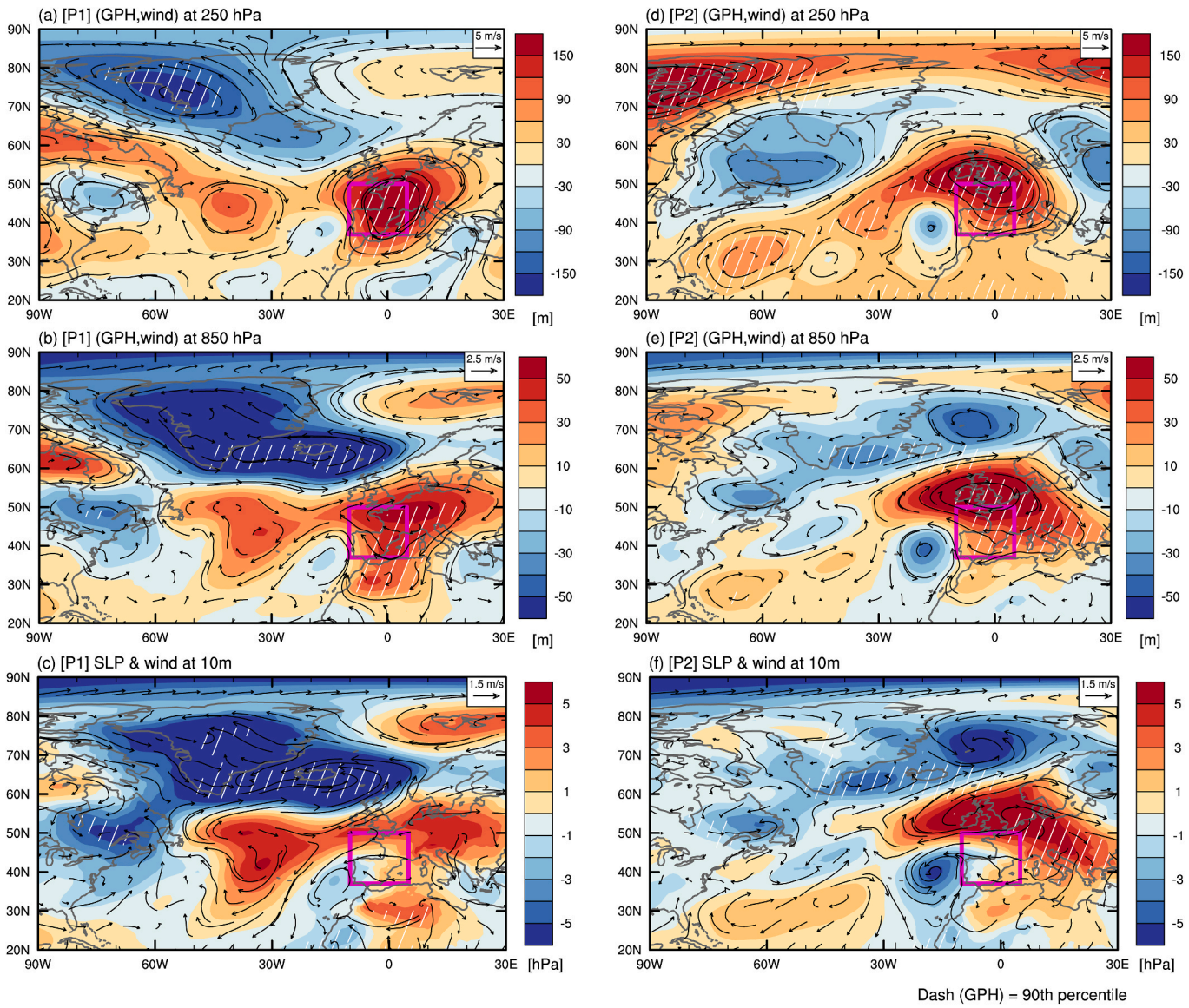

Fig. 5. (a–b) Anomalies of geopotential height (GPH; shaded; unit: m), wind (vector; unit: m/s) at 250 hPa and 850 hPa, (c) mean sea level pressure (SLP), and wind at 10 m during P1. (d–f) The same as in panels a–c, but for P2. The white dashed patterns indicate above the 90th percentile for the analysis period. The pink rectangle indicates a SWEU region. (For interpretation of the references to color in this figure legend, the reader is referred to the Web version of this article.)

Stream region likely played a crucial role in shaping the atmospheric circulation patterns that contributed to the 2022 SWEU-HW. These SST anomalies can enhance atmospheric instability by increasing convection and latent heat release, which warms the atmosphere and amplifies stationary Rossby waves, favoring the development and persistence of stationary high-pressure systems. This mechanism is consistent with the findings of Mathews et al. (2024), who demonstrated that anomalous warm SSTs in the Gulf Stream region could drive atmospheric responses that amplify the atmospheric blocking events and lead to extreme weather conditions, including HWs. Such interactions suggest the feedback where warm SSTs in the Gulf Stream enhance atmospheric blocking and prolong HW conditions. This result implies that the warm SSTs in the Gulf Stream were amplified in 2022, which may have played an essential role in causing atmospheric circulation patterns favorable for developing the 2022 SWEU-HW, as Palter (2015) suggested.

Next, we investigated whether the unusually warm SST of the Gulf Stream caused the 2022 SWEU-HW through a global climate modeling experiment using CESM v1.2.2. The results confirmed the difference in the atmospheric response by prescribing the SST anomaly to the Gulf Stream in the NA from June to July 2022, when the SST was unusually high (Fig. 7). When an increased NA-SST was prescribed, stagnant anticyclones over the SWEU region strongly developed in the upper and lower troposphere (Fig. 8). The cross-section along the line indicates that anomalous high pressure and air temperature significantly increased in the SWEU region. These atmospheric circulation patterns, favorable to the 2022 SWEU-HW, remarkably resembled the reanalysis data analysis results. Although the modeling experiments revealed atmospheric circulation patterns favorable for the 2022 SWEU-HW, there was no statistically significant increase in the surface temperature. This may be due to various causes, such as limitations in air–sea heat exchange and regional temperature changes, including differences in responses, model sensitivity, and feedback mechanisms. In particular, differences in regional temperature responses may have been insufficient to have a noticeable effect on the surface temperatures in these regions, even if SST changes affected the atmospheric circulation patterns over the IP and SWEU. Various regional and global climate factors and SST can influence local temperatures. Nevertheless, the modeling experiments demonstrated that abnormal upper troposphere

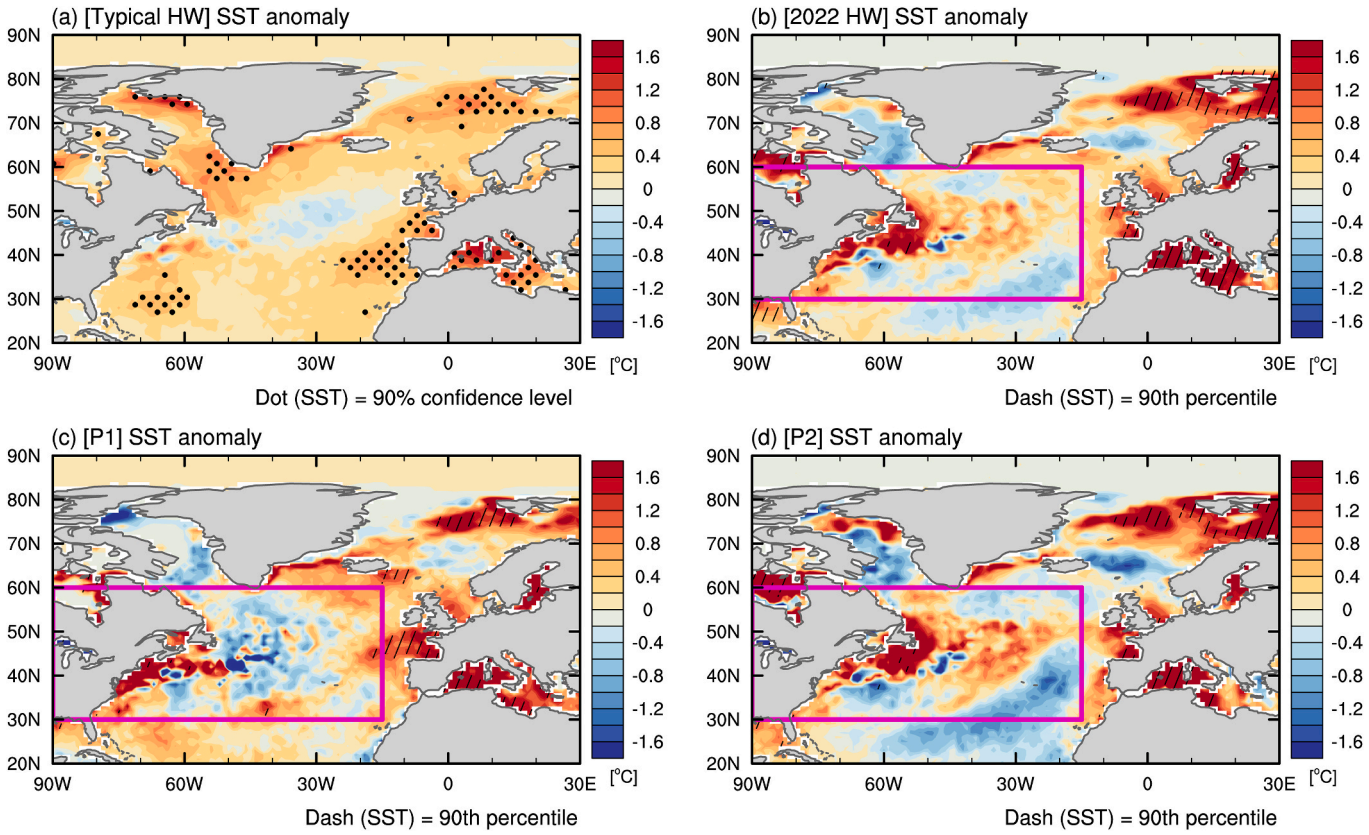

Fig. 6. (a) Composite anomaly patterns for sea surface temperature (SST; shaded; unit: °C) in typical SWEU-HWs during June-July. (a) The black dots indicate statistically significant values at the 90% level. (b) SST anomaly pattern in 2022 SWEU-HW during June-July. (c–d) Same as in Fig. 6(b), but for during P1 and P2, respectively. The black dashed patterns indicate above the 90th percentile from the analysis period. Pink rectangles indicate the Gulf Stream region. (For interpretation of the references to color in this figure legend, the reader is referred to the Web version of this article.)

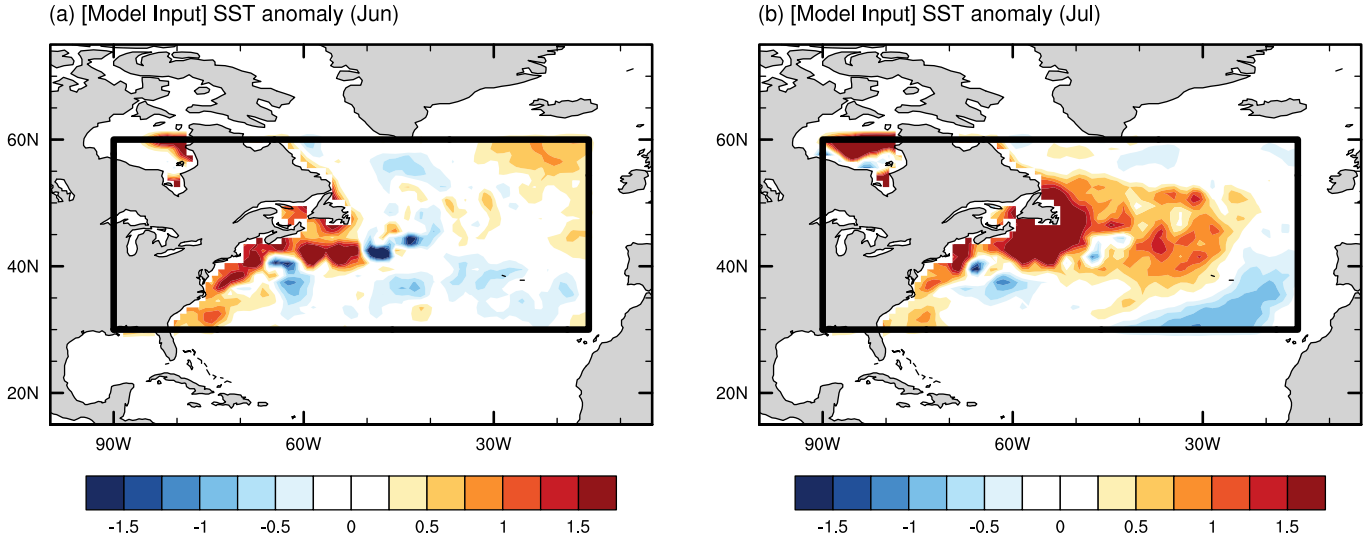

Fig. 7. (a–b) Prescribed SST anomaly (units: °C) forcings from CESM model experiments for June–July. The black rectangle region (30° N–60° N, 90° W–15° W) indicates a prescribed SST forcing region.

atmospheric blocking in the atmospheric circulation pattern associated with the extreme HWs in the SWEU was closely related to the strengthening of the Gulf Stream warm SST anomalies.

4. Discussion and conclusions

We investigated the physical processes and mechanisms that caused the HWs in SWEU during the early summer (June to July) in 2022. According to the analyzed dataset, the 2022 SWEU-HW was the most extreme HW in the past 43 years, while tree-ring proxy data from Büntgen et al. (2024) reported it as the most extreme HW in the last 900 years. Importantly, the 2022 SWEU-HW showed a clearly different atmospheric circulation pattern from typical SWEU HWs. While typical SWEU-HWs are affected by wavy atmospheric patterns, the 2022

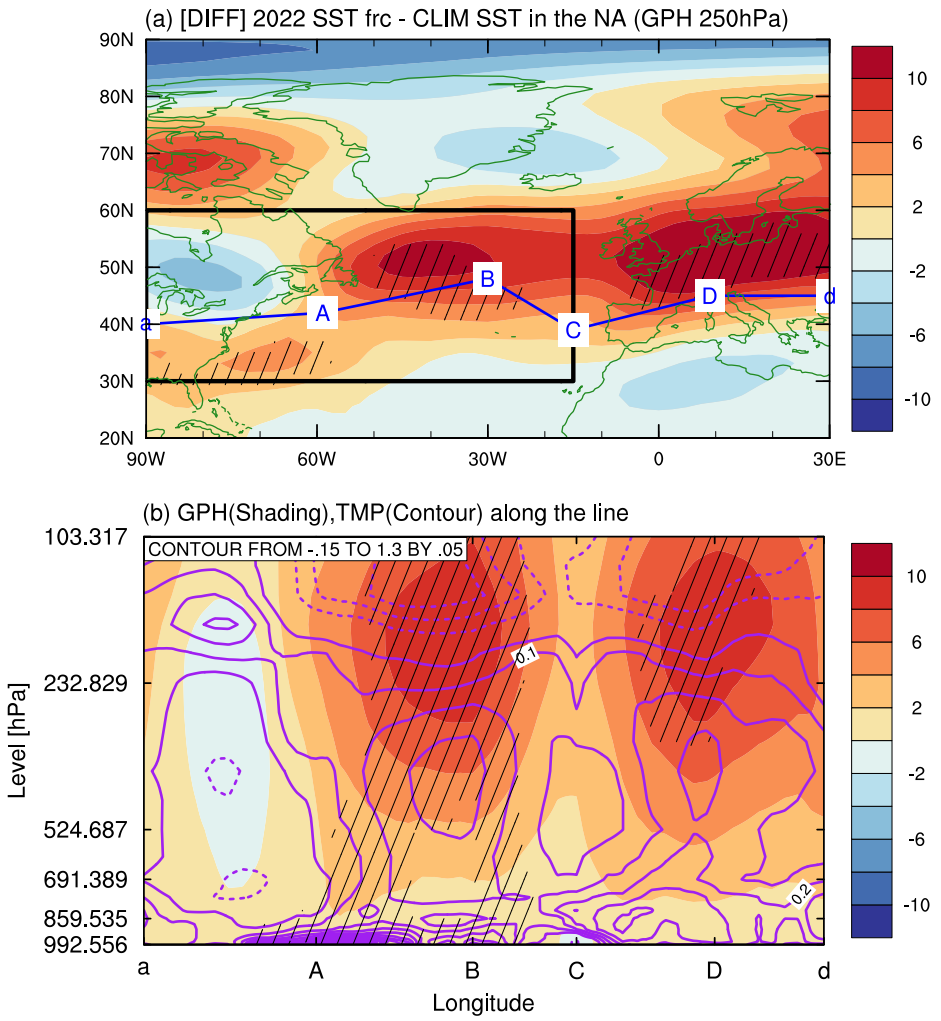

Fig. 8. Model responses of the increased SST in the NA (black rectangle) for (a) spatial pattern of geopotential height (GPH) at 250 hPa (unit: m) and (b) the vertical cross-section of GPH (shaded; unit: m). (b) Vertical cross-section of air temperature (TMP; purple contours; unit: °C) along the line in Fig. 8(a). The model responses are calculated as a difference between the SSTexp and CTRL. The hatched area denotes statistically significant values at 90%. The blue line connecting points a through d is the same as shown in Fig. 2b, indicating the pathway of the atmospheric feature being analyzed. (For interpretation of the references to color in this figure legend, the reader is referred to the Web version of this article.)

SWEU-HW was strongly affected by a stagnant high-pressure anomaly.

During the 2022 SWEU-HWs, extreme temperature increases occurred in June and July, respectively, and anticyclonic anomalies with barotropic structures and lower troposphere heat domes were evident. Regarding the physical process, temperatures in SWEU increased mainly due to a combination of weakened cold air advection from the ocean, increased warm air advection from the African continent, and adiabatic heating. This pattern of warm air advection was consistent with findings by Serrano-Notivoli et al. (2023), who attributed the HW to a blocking event in the NA region that promoted the northward movement of hot air masses from Africa towards the IP. In addition, shortwave radiation at the surface increased due to strong anticyclonic anomalies, and the increased radiant energy was mainly dissipated via longwave radiation and sensible heat flux. In addition, there was a significant difference in specific humidity between P1 and P2, with P1 being relatively warm and humid and P2 having warm and dry atmospheric conditions. As a result, the DLW increased during P1, whereas no changes were observed in P2.

Our investigation of the causes of the atmospheric circulation patterns related to the 2022 SWEU-HWs revealed that abnormal atmospheric blocking in the upper troposphere mainly caused the extreme HWs in P1 and P2. Particularly, the atmospheric blocking in the summer of 2022 was closely associated with the amplification of the Gulf Stream SST, which caused an atmospheric circulation pattern favorable for the 2022 SWEU-HWs, as revealed by modeling experiments.

Our results reveal that anomalous warm SSTs play a crucial role in driving HWs in SWEU, simliar to findings from the 2003 European HW. The 2003 HW has been extensively analyzed, with several studies highlighting the primary role of SSTs in the Mediterranean Sea (Feudale and Shukla, 2011; Garcia-Herrera et al., 2010b; Xoplaki et al., 2003). In contrast, the extreme HW in 2022 SWEU exhibited different characteristics. Our study highlights that the amplification of the Gulf Stream in the NA primarily drove the 2022 SWEU. This significant finding differentiates the 2022 event from typical HWYs, where Mediterranean SST anomalies were the primary drivers.

The primary goal of this study is not to attribute the observed 2022 SWEU-HW directly to climate change, although this could be a focus of future research. Interestingly, most extreme HW events over the past 20 years have been more frequent and intense. In fact, recent research utilizing tree-ring proxy data indicates that the summer warming over the western Mediterranean region has been unprecedented since medieval times (Büntgen et al., 2024). This raises the question: why is this happening? One potential explanation could be the warming of SSTs in the Atlantic Ocean and Mediterranean Sea, which deserves further investigation and hypothesis generation based on current data and trends observed in other studies. This finding is consistent with prior research, which has shown the extreme nature of recent HWs, including

the notable 2022 event that appears to surpass the intensity of the previous HWs.

In this study, we only considered one HWY, i.e., 2022. It is important to recognize that the extreme nature of such an event makes it highly challenging to draw definite conclusions from the reanalysis dataset. Nevertheless, this study demonstrated the physical process and potential mechanism of the 2022 SWEU-HW through statistical analysis and model experiments. The results of this study emphasize that a Gulf Stream SSTs amplification can trigger an atmospheric circulation pattern favorable for extreme HWs in SWEU. This study advances the understanding of HW dynamics by improving previous research methodologies. However, it is essential to acknowledge the limitations, such as the model's inability to capture these events' complexity fully. Future research should focus on refining these models and exploring additional variables that could enhance predictive accuracy. Studies should investigate the long-term trends and drivers of HWs, particularly the influence of SSTs and other climatic factors like the Gulf Stream. Wills et al. (2016) highlighted that Gulf Stream SST variability significantly influences North Atlantic atmospheric circulation, affecting long-term weather patterns. Small et al. (2014) demonstrated that changes in ocean fronts, including the Gulf Stream, can modify storm track behavior and intensity, which is essential for future climate scenarios. Lee et al. (2018) showed that Gulf Stream SST biases can cause shifts in global atmospheric circulation due to long-term SST changes. Kelly et al. (2010) suggested that interactions between the Gulf Stream and the atmosphere could impact mid-latitude storm tracks and atmospheric blocking under changing climate conditions. Mathews et al. (2024) found that variations in Gulf Stream latent heat fluxes modulate the atmospheric blocking frequency, influencing the occurrence and intensity of HWs. These findings emphasize the importance of understanding current variability and projected changes in Gulf Stream dynamics to improve climate models, thereby enhancing the forecasting of sub-seasonal HWs and projections in global climate models.

CRediT authorship contribution statement

Jeong-Hun Kim: Writing – original draft, Methodology, Investigation, Formal analysis, Data curation, Conceptualization. **So-Hyun Nam:** Writing – review & editing, Visualization, Formal analysis, Data curation. **Maeng-Ki Kim:** Writing – review & editing, Methodology, Investigation, Conceptualization. **Roberto Serrano-Notivoli:** Writing – review & editing, Investigation. **Ernesto Tejedor:** Writing – review & editing, Investigation.

Declaration of competing interest

The authors declare that they have no known competing financial interests or personal relationships that could have appeared to influence the work reported in this paper.

Data availability

Data will be made available on request.

Acknowledgments

This work was funded by Korea Meteorological Administration (KMA) Research and Development Program under Grant KMI2022-01311 and the Specialized university program for confluence analysis of Weather and Climate Data of the KMI funded by the Korean government (KMA). RSN is supported by grant RYC2021-034330-I funded by MCIN/AEI/10.13039/501100011033 and by "European Union NextGenerationEU/PRTR". ET is funded by the Community of Madrid through the grant "2023-T1/ECO-29118." The authors thank Seul-Ah Kim (http://orcid.org/0009-0004-6209-4548), Eun-Gyu Park (http://orcid.org/0009-0008-5149-6321), and Ha-Eun Kim (http://orcid.org/0009-0000-9899-1356) for their help in designating and discussing the research topic.

References

Barriopedro, D., Fischer, E.M., Luterbacher, J., Trigo, R.M., García-Herrera, R., 2011. The hot summer of 2010: redrawing the temperature record map of Europe. Science 332, 220–224. https://doi.org/10.1126/science.1201224, 1979.

Barriopedro, D., García-Herrera, R., Ordóñez, C., Miralles, D.G., Salcedo-Sanz, S., 2023. Heat waves: physical understanding and scientific challenges. Rev. Geophys. 61. https://doi.org/10.1029/2022RG000780.

Bento, V.A., Russo, A., Gouveia, C.M., Dacamara, C.C., 2022. Recent change of burned area associated with summer heat extremes over Iberia. Int. J. Wildland Fire 31, 658–669. https://doi.org/10.1071/WF21155.

Büntgen, U., Reinig, F., Verstege, A., Piermattei, A., Kunz, M., Krusic, P., Slavin, P., Štěpánek, P., Torbenson, M., del Castillo, E.M., Arosio, T., Kirdyanov, A., Oppenheimer, C., Trnka, M., Palosse, A., Bebchuk, T., Camarero, J.J., Esper, J., 2024. Recent summer warming over the western Mediterranean region is unprecedented since medieval times. Global Planet. Change 232. https://doi.org/10.1016/j.gloplacha.2023.104336.

Duchez, A., Frajka-Williams, E., Josey, S.A., Evans, D.G., Grist, J.P., Marsh, R., McCarthy, G.D., Sinha, B., Berry, D.I., Hirschi, J.J.M., 2016. Drivers of exceptionally cold North Atlantic Ocean temperatures and their link to the 2015 European heat wave. Environ. Res. Lett. 11. https://doi.org/10.1088/1748-9326/11/7/074004.

Feudale, L., Shukla, J., 2011. Influence of sea surface temperature on the European heat wave of 2003 summer. Part I: an observational study. Clim. Dynam. 36, 1691–1703. https://doi.org/10.1007/s00382-010-0788-0.

Fischer, E.M., Schär, C., 2010. Consistent geographical patterns of changes in high-impact European heatwaves. Nat. Geosci. 3, 398–403. https://doi.org/10.1038/ngeo866.

Folland, C.K., Knight, J., Linderholm, H.W., Fereday, D., Ineson, S., Hurrel, J.W., 2009. The summer North Atlantic oscillation: past, present, and future. J. Clim. 22, 1082–1103. https://doi.org/10.1175/2008JCLI2459.1.

Garcia-Herrera, R., Díaz, J., Trigo, R.M., Luterbacher, J., Fischer, E.M., 2010a. A review of the european summer heat wave of 2003. Crit. Rev. Environ. Sci. Technol. https://doi.org/10.1080/10643380802238137.

Garcia-Herrera, R., Díaz, J., Trigo, R.M., Luterbacher, J., Fischer, E.M., 2010b. A review of the european summer heat wave of 2003. Crit. Rev. Environ. Sci. Technol. https://doi.org/10.1080/10643380802238137.

Hersbach, H., Bell, B., Berrisford, P., Hirahara, S., Horányi, A., Muñoz-Sabater, J., Nicolas, J., Peubey, C., Radu, R., Schepers, D., Simmons, A., Soci, C., Abdalla, S., Abellan, X., Balsamo, G., Bechtold, P., Biavati, G., Bidlot, J., Bonavita, M., De Chiara, G., Dahlgren, P., Dee, D., Diamantakis, M., Dragani, R., Flemming, J., Forbes, R., Fuentes, M., Geer, A., Haimberger, L., Healy, S., Hogan, R.J., Hólm, E., Janisková, M., Keeley, S., Laloyaux, P., Lopez, P., Lupu, C., Radnoti, G., de Rosnay, P., Rozum, I., Vamborg, F., Villaume, S., Thépaut, J.N., 2020. The ERA5 global reanalysis. Q. J. R. Meteorol. Soc. 146, 1999–2049. https://doi.org/10.1002/qj.3803.

Kelly, K.A., Small, R.J., Samelson, R.M., Qiu, B., Joyce, T.M., Kwon, Y.O., Cronin, M.F., 2010. Western boundary currents and frontal air-sea interaction: gulf stream and Kuroshio Extension. J. Clim. 23, 5644–5667. https://doi.org/10.1175/2010JCLI3346.1.

Kim, Jeong Hun, Kim, S.J., Kim, Joo Hong, Hayashi, M., Kim, M.K., 2022. East Asian heatwaves driven by Arctic-Siberian warming. Sci. Rep. 12. https://doi.org/10.1038/s41598-022-22628-9.

Kim, M.K., Oh, J.S., Park, C.K., Min, S.K., Boo, K.O., Kim, J.H., 2019. Possible impact of the diabatic heating over the Indian subcontinent on heat waves in South Korea. Int. J. Climatol. 39, 1166–1180. https://doi.org/10.1002/joc.5869.

Lee, R.W., Woollings, T.J., Hoskins, B.J., Williams, K.D., O'Reilly, C.H., Masato, G., 2018. Impact of Gulf Stream SST biases on the global atmospheric circulation. Clim. Dynam. 51, 3369–3387. https://doi.org/10.1007/s00382-018-4083-9.

Li, M., Yao, Y., Simmonds, I., Luo, D., Zhong, L., Chen, X., 2020. Collaborative impact of the nao and atmospheric blocking on european heatwaves, with a focus on the hot summer of 2018. Environ. Res. Lett. 15. https://doi.org/10.1088/1748-9326/aba6ad.

Liu, X., He, B., Guo, L., Huang, L., Chen, D., 2020. Similarities and differences in the mechanisms causing the European summer heatwaves in 2003, 2010, and 2018. Earth's Future 8. https://doi.org/10.1029/2019EF001386.

Mathews, J.P., Czaja, A., Vitart, F., Roberts, C., 2024. Gulf stream moisture fluxes impact atmospheric blocks throughout the northern hemisphere. Geophys. Res. Lett. 51. https://doi.org/10.1029/2024GL108826.

Miralles, D.G., Teuling, A.J., Van Heerwaarden, C.C., De Arellano, J.V.G., 2014. Mega-heatwave temperatures due to combined soil desiccation and atmospheric heat accumulation. Nat. Geosci. 7, 345–349. https://doi.org/10.1038/ngeo2141.

Palter, J.B., 2015. The role of the gulf stream in European climate. Ann. Rev. Mar. Sci 7, 113–137. https://doi.org/10.1146/annurev-marine-010814-015656.

Robine, J.M., Cheung, S.L.K., Le Roy, S., Van Oyen, H., Griffiths, C., Michel, J.P., Herrmann, F.R., 2008. Death toll exceeded 70,000 in Europe during the summer of 2003. C R Biol. 331, 171–178. https://doi.org/10.1016/j.crvi.2007.12.001.

Rousi, E., Kornhuber, K., Beobide-Arsuaga, G., Luo, F., Coumou, D., 2022. Accelerated western European heatwave trends linked to more-persistent double jets over Eurasia. Nat. Commun. 13. https://doi.org/10.1038/s41467-022-31432-y.

Sánchez-Benítez, A., García-Herrera, R., Barriopedro, D., Sousa, P.M., Trigo, R.M., 2018. 2017: the earliest European summer mega-heatwave of reanalysis period. Geophys. Res. Lett. 45, 1955–1962. https://doi.org/10.1002/2018GL077253.

Seneviratne, S.I., Corti, T., Davin, E.L., Hirschi, M., Jaeger, E.B., Lehner, I., Orlowsky, B., Teuling, A.J., 2010. Investigating soil moisture-climate interactions in a changing climate: a review. Earth Sci. Rev. https://doi.org/10.1016/j.earscirev.2010.02.004.

Seo, E., Lee, M.I., Jeong, J.H., Koster, R.D., Schubert, S.D., Kim, H.M., Kim, D., Kang, H. S., Kim, H.K., MacLachlan, C., Scaife, A.A., 2019. Impact of soil moisture initialization on boreal summer subseasonal forecasts: mid-latitude surface air temperature and heat wave events. Clim. Dynam. 52, 1695–1709. https://doi.org/10.1007/s00382-018-4221-4.

Serrano-Notivoli, R., Lemus-Canovas, M., Barrao, S., Sarricolea, P., Meseguer-Ruiz, O., Tejedor, E., 2022. Heat and cold waves in mainland Spain: origins, characteristics, and trends. Weather Clim. Extrem. 37. https://doi.org/10.1016/j.wace.2022.100471.

Serrano-Notivoli, R., Tejedor, E., Sarricolea, P., Meseguer-Ruiz, O., de Luis, M., Saz, M.Á., Longares, L.A., Olcina, J., 2023. Unprecedented warmth: a look at Spain's exceptional summer of 2022. Atmos. Res. https://doi.org/10.1016/j.atmosres.2023.106931.

Simmonds, I., Govekar, P.D., 2014. What are the physical links between Arctic sea ice loss and Eurasian winter climate? Environ. Res. Lett. https://doi.org/10.1088/1748-9326/9/10/101003.

Small, R.J., Tomas, R.A., Bryan, F.O., 2014. Storm track response to ocean fronts in a global high-resolution climate model. Clim. Dynam. 43, 805–828. https://doi.org/10.1007/s00382-013-1980-9.

Son, J.H., Kim, N.H., Kim, G.U., Chu, J.E., Park, J.H., Kwon, J. Il, Heo, K.Y., 2022. Early-onset trend in European summer caused by Greenland topographic effect. Environ. Res. Lett. 17. https://doi.org/10.1088/1748-9326/ac94e7.

Sousa, P.M., Trigo, R.M., Barriopedro, D., Soares, P.M.M., Santos, J.A., 2018. European temperature responses to blocking and ridge regional patterns. Clim. Dynam. 50, 457–477. https://doi.org/10.1007/s00382-017-3620-2.

Stéfanon, M., Drobinski, P., D'Andrea, F., Lebeaupin-Brossier, C., Bastin, S., 2014. Soil moisture-temperature feedbacks at meso-scale during summer heat waves over Western Europe. Clim. Dynam. 42, 1309–1324. https://doi.org/10.1007/s00382-013-1794-9.

Takaya, K., Nakamura, H., 2001. A formulation of a phase-independent wave-activity flux for stationary and migratory quasigeostrophic eddies on a zonally varying basic flow. J. Atmos. Sci. 58, 608–627. https://doi.org/10.1175/1520-0469(2001)058<0608:AFOAPI>2.0.CO;2.

Tejedor, E., Benito, G., Serrano-Notivoli, R., González-Rouco, F., Esper, J., Büntgen, U., 2024. Recent heatwaves as a prelude to climate extremes in the western Mediterranean region. NPJ. Clim. Atmos. Sci. 7, 218. https://doi.org/10.1038/s41612-024-00771-6.

Tomczyk, A.M., Półrolniczak, M., Bednorz, E., 2017. Circulation conditions' effect on the occurrence of heatwaves in Western and Southwestern Europe. Atmosphere 8. https://doi.org/10.3390/atmos8020031.

Toreti, A., Bavera, D., Acosta Navarro, J., Arias Muñoz, C., Barbosa, P., De Jager, A., Di Ciollo, C., Fioravanti, G., Hrast Essenfelder, A., Maetens, W., Magni, D., Masante, D., Mazzeschi, M., McCormick, N., Salamon, P., European Commission. Joint Research Centre, 2023. Drought in Europe : August 2023 : GDO Analytical Report.

Tripathy, K.P., Mishra, A.K., 2023. How unusual is the 2022 European compound drought and heatwave event? Geophys. Res. Lett. 50. https://doi.org/10.1029/2023GL105453.

Vautard, R., Van Aalst, M., Boucher, O., Drouin, A., Haustein, K., Kreienkamp, F., Van Oldenborgh, G.J., Otto, F.E.L., Ribes, A., Robin, Y., Schneider, M., Soubeyroux, J.M., Stott, P., Seneviratne, S.I., Vogel, M.M., Wehner, M., 2020. Human contribution to the record-breaking June and july 2019 heatwaves in western Europe. Environ. Res. Lett. 15. https://doi.org/10.1088/1748-9326/aba3d4.

Wills, S.M., Thompson, D.W.J., Ciasto, L.M., 2016. On the observed relationships between variability in gulf stream sea surface temperatures and the atmospheric circulation over the North Atlantic. J. Clim. 29, 3719–3730. https://doi.org/10.1175/JCLI-D-15-0820.1.

Xoplaki, E., González-Rouco, J.F., Luterbacher, J., Wanner, H., 2003. Mediterranean summer air temperature variability and its connection to the large-scale atmospheric circulation and SSTs. Clim. Dynam. 20, 723–739. https://doi.org/10.1007/s00382-003-0304-x.

Yanai, M., Esbensen, S., Chu, J.-H., 1973. Determination of bulk properties of tropical cloud clusters from large-scale heat and moisture budgets. J. Atmos. Sci. 30, 611–627. https://doi.org/10.1175/1520-0469(1973)030<0611:DOBPOT>2.0.CO;2.